Structural Durability & Health Monitoring

Tech Science Press

https://doi.org/10.32604/sdhm.2026.079206

ARTICLE

# Corrosion Behavior of Natural Gas Pipeline Steel in Acidic Red Soil Environments of Southern Jiangxi

**Siwen Liu[1,2,3], Ke Mei[2,3], Shiyao Zhu[2,3], Ruiquan Liao[1,2,3,*] and Xuyu Liu[4]**

[1]State Key Laboratory of Low Carbon Catalysis and Carbon Dioxide Utilization, Wuhan, China
[2]Hubei Key Laboratory of Oil and Gas Drilling and Production Engineering, Yangtze University, Wuhan, China
[3]School of Petroleum Engineering, Yangtze University, Wuhan, China
[4]The Third Oil Transmission Department of PetroChina Changqing Oilfield Company, Yinchuan, China

*Corresponding Author: Ruiquan Liao. Email: liaoruiquan@263.net

Received: 16 January 2026; Accepted: 02 April 2026; Published: 30 June 2026

**ABSTRACT:** Acidic red soil is widely distributed in southern Jiangxi and exhibits strong corrosivity, posing a significant threat to buried pipeline steels. In this work, six acidic red soil samples collected from this region were analyzed in terms of their physicochemical characteristics using pH testing and ion chromatography, and corresponding simulated soil solutions were prepared. The corrosion behavior of L415 pipeline steel in these solutions was systematically evaluated through immersion weight-loss experiments, potentiodynamic polarization, electrochemical impedance spectroscopy (EIS), scanning electron microscopy (SEM), and X-ray diffraction (XRD). All six soil solutions were found to be acidic. Variations in corrosion rate were primarily controlled by pH and ionic concentration. Lower pH values and higher ion contents resulted in more severe corrosion. The dominant corrosion products in all environments were identified as $Fe_3O_4$ and FeOOH. Electrochemical analysis further revealed the combined and complex effects of different ionic species on the corrosion mechanism of L415 steel in acidic red soil solutions. The findings of this study provide a theoretical basis for corrosion protection strategies of buried natural gas pipelines in acidic red soil regions.

**KEYWORDS:** L415 pipeline steel; acidic red soil; soil corrosion; electrochemical curve

## 1 Introduction

Pipeline transportation has become a widely adopted mode for oil and gas delivery owing to its large transport capacity, high economic efficiency, and superior safety performance [1]. Oil and gas pipelines are typically buried deep underground and therefore continuously face corrosion risks arising from the surrounding soil environment during service [2]. Soil corrosion of pipeline steels is governed by multiple complex factors, including ionic concentration, pH, dissolved oxygen, and microbial activity [3–5]. Xie et al. [6] investigated the electrochemical corrosion behavior of X70 steel in simulated Liaohe oilfield soil solution under the combined effects of dissolved oxygen, $HCO_3^-$, and $Cl^-$ using an orthogonal experimental design. Their results indicated that among the three factors, $Cl^-$ exhibited the weakest corrosive effect, whereas $HCO_3^-$ had the most significant influence on the corrosion behavior of X70 steel. Xu et al. [7] studied the effect of dissolved oxygen on the corrosion behavior of X70 pipeline steel in a low-temperature acidic bentonite-based simulated soil solution and found that under low dissolved oxygen conditions, the corrosion product film became denser and provided enhanced protection to the steel substrate. Setiawan et al. [8] investigated the corrosion behavior of X60 steel in Indonesian soils with varying ammonium

sulfate concentrations and pH values, revealing that the corrosion rate increased with increasing pH but decreased with increasing ammonium sulfate concentration. Fu et al. [9] examined the influence of nitrate-reducing bacteria on the corrosion behavior of X80 pipeline steel in soil leachate from the Shenyang region and concluded that nitrate-reducing bacteria accelerated the corrosion rate of the steel and promoted the formation of pitting corrosion on the steel surface [10–12].

Under the strategic initiatives of "Gasification of Jiangxi" and "Long-Distance Natural Gas Transmission to Every County", a large number of natural gas pipelines have been constructed in the southern Jiangxi region. The soils in this area are predominantly red soils, which are characterized by a deficiency of alkali and alkaline earth metals but are enriched in iron and aluminum oxides [13]. These soils generally exhibit pH values in the range of 4–6 and display a typical acidic red appearance. Acidic red soils can significantly accelerate metal corrosion, thereby posing a serious threat to the safe operation of buried pipelines. Therefore, systematic investigations into the corrosion behavior of natural gas pipelines in acidic red soil environments in southern Jiangxi are of great theoretical significance and practical engineering value [14–18].

Cao et al. [10] investigated the corrosion behavior of X80 pipeline steel welded joints in acidic red soil solution and reported that uniform corrosion occurred on the weld surface after 840 h of immersion, with the heat-affected zone exhibiting more severe corrosion than both the base metal and the weld metal. Wei et al. [11] compared the alternating current corrosion behavior of X80 steel in real soil, soil leachate, and simulated solutions, and found that the AC corrosion (Alternating current corrosion) behavior in soil leachate more closely resembled that in actual soil environments. In addition, Li et al. [19] comparatively analyzed the corrosion characteristics of Q235 steel in saturated acidic red soil and yellow soil, revealing that the lower pH, higher concentration of aggressive anions, and the presence of high-valence iron oxides in red soil resulted in higher corrosion rates and greater susceptibility to localized corrosion [20].

L415 pipeline steel is a low-carbon, low-alloy high-strength steel that exhibits excellent weldability, high strength, and good toughness, making it well suited for high-pressure and long-distance oil and gas transportation [13,21–23]. Wan et al. found that the corrosion of L415 pipeline steel in solutions with low ionic concentrations was dominated by pitting corrosion. When the ionic concentration increased to ten times that of the original solution, the corrosion mode of the pipeline steel transformed into uniform corrosion [24–26]. In Jiangxi Province, the majority of provincially operated natural gas pipelines are constructed using L415 steel [2,27,28]. Therefore, investigating the corrosion resistance of L415 pipeline steel in acidic red soil environments is of great importance for ensuring the operational safety of pipelines in the southern Jiangxi region. In this study, soils from the southern Jiangxi region were systematically characterized, and the corrosion behavior of L415 pipeline steel in simulated soil solutions was investigated through immersion tests and electrochemical measurements. Based on the experimental results, the corrosion characteristics of pipeline steel in acidic red soil environments were elucidated, and the underlying corrosion mechanisms were analyzed.

## 2 Experimental Materials and Methods

### *2.1 Experimental Material and Physicochemical Characterization of Soil*

L415 pipeline steel was selected as the experimental material in this study. As illustrated in Fig. 1, its microstructure mainly consists of ferrite and pearlite (F + P). Six acidic red soil samples were collected at a depth of approximately 1 m near cathodic protection test stations in southern Jiangxi. The samples were labeled D100, D200, D300, S100, S200, and S300. After removing debris and impurities, the soils were crushed, ground, sieved, and dried. Each processed soil sample was mixed with deionized water at a mass ratio of 1:10. The mixtures were shaken at 200 rpm and 30°C for 30 min and then allowed to stand for

12 h to achieve solid–liquid separation. The supernatant was subsequently extracted and analyzed using ion chromatography and a pH meter to determine ionic concentrations and pH values.

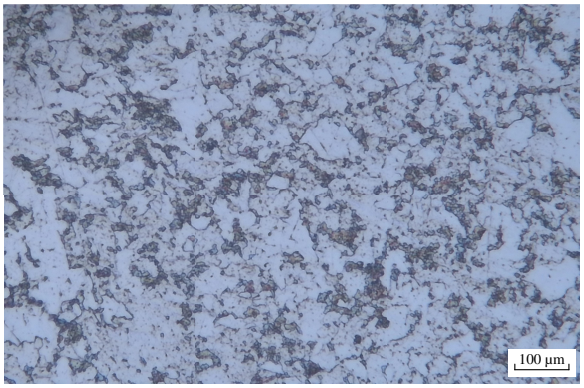


**Figure 1:** Metallographic microstructure of L415 pipeline steel.

It should be noted that the soil extract solutions prepared using the 1:10 soil–water mixing method were employed as a simplified and controlled representation of the soil environment. This approach is widely used to evaluate the relative corrosivity of different soils by isolating the effects of pH, ionic composition, and electrical conductivity. However, the simulated soil solution cannot fully reproduce the complexity of real buried soil environments, such as soil heterogeneity, moisture gradients, oxygen diffusion limitations, and microbial activity. Therefore, the results obtained in this study are mainly intended for qualitative corrosion risk assessment and comparative ranking of different soil environments, rather than for direct quantitative prediction of in-service corrosion rates of buried pipelines.

### *2.2 Electrochemical Measurements*

Electrochemical tests were carried out using a CHI760E workstation with a conventional three-electrode configuration. L415 pipeline steel served as the working electrode, a graphite rod acted as the counter electrode, and a saturated calomel electrode (SCE) was used as the reference electrode.

Specimens were prepared by wire cutting into dimensions of 10 mm × 10 mm × 3 mm. Each sample was connected to a copper wire, leaving an exposed working surface area of 1 $cm^2$, while the remaining surfaces were sealed with epoxy resin. Prior to testing, the working surfaces were sequentially polished with silicon carbide papers up to 1200 grit, rinsed with deionized water, and immersed in the respective simulated soil solutions.

After immersion for 14 days, the specimens were removed and subjected to open circuit potential (OCP) measurements. Once a stable OCP was achieved, electrochemical impedance spectroscopy (EIS) tests were conducted for each specimen over a frequency range of 0.01 Hz to $1 \times 10^5$ Hz, with an AC perturbation amplitude of 10 mV. Potentiodynamic polarization measurements were subsequently carried out with a potential scanning range from −1.2 to −0.2 V at a scan rate of 0.5 mV/s.

### *2.3 Weight-Loss Tests and Corrosion Morphology Analysis*

L415 pipeline steel was cut into specimens with dimensions of 40 mm × 13 mm × 2 mm. All six surfaces of the specimens were sequentially ground using silicon carbide abrasive papers up to 1200-grit. The specimens were then rinsed with deionized water, dried, and weighed. Subsequently, the specimens were immersed in six different soil solutions for 14 days. After the designated immersion period, the specimens were removed

from the solutions and sequentially dehydrated in absolute ethanol with volume fractions of 20%, 40%, 80%, and 100%. The corrosion products on the specimen surfaces were then removed using a chemical rust remover. Afterward, the specimens were rinsed with deionized water, dried with compressed air, and placed in a drying oven for 24 h to ensure complete drying. The specimens were finally weighed, and the corrosion rate of L415 pipeline steel, $v_{corr}$, was calculated according to the following equation:

$$v_{corr} = \frac{K\,(m_0 - m_1)}{S \cdot t \cdot \rho} \tag{1}$$

In the equation, $K$ is a constant with a value of 87,600; $m_0$ and $m_1$ represent the masses of the specimens before and after immersion, respectively; $S$ is the exposed surface area; $t$ is the immersion time; and $\rho$ is the density of the steel.

After immersion, the corrosion morphologies of the specimens were observed using scanning electron microscopy (SEM). The corrosion products were carefully scraped off and collected, and their phase compositions were analyzed by X-ray diffraction (XRD).

## 3 Results and Discussion

### *3.1 Corrosion Rate and Morphology Analysis*

The ionic concentrations and pH values of the six soil extract solutions are summarized in Table 1. Fig. 2 presents the calculated corrosion rates of L415 pipeline steel after immersion in the different simulated soil solutions. The corrosion rates of the specimens decrease in the following order: S100 > D300 > D100 > D200 > S200 > S300.

**Table 1:** Ionic concentrations and pH values of soil solutions.

| Sample ID | $Na^+$ (mg/L) | $K^+$ (mg/L) | $Mg^{2+}$ (mg/L) | $Cl^-$ (mg/L) | $SO_4^{2-}$ (mg/L) | $NO_3^-$ (mg/L) | $HCO_3^-$ (mg/L) | pH |
|---|---|---|---|---|---|---|---|---|
| D100 | 4.61 | 6.31 | 1.45 | 18.24 | 5.03 | 3.24 | 0.55 | 3.83 |
| D200 | 8.57 | 8.46 | 1.06 | 29.91 | 2.71 | 2.1 | 12.64 | 4.92 |
| D300 | 6.09 | 16.6 | 6.94 | 5.82 | 56.57 | 3.37 | 0.55 | 3.29 |
| S100 | 6.73 | 40.97 | 14.24 | 5.6 | 243.66 | 86.37 | 11.6 | 4.11 |
| S200 | 6.23 | 16.82 | 1.8 | 8.69 | 12.03 | 9.55 | 15.26 | 5.58 |
| S300 | 8.23 | 31.53 | 7.67 | 12.34 | 27.97 | 2.03 | 20.97 | 5.33 |

As shown in Fig. 2, the corrosion rates of the specimens in soil solutions S100, D300, and D100 are significantly higher than those in the other solutions. Among them, the corrosion rate in the S100 solution is the highest, reaching 0.1949 mm/a, which is approximately 4.3 times that in the solution with the lowest corrosion rate (S300). According to the physicochemical properties of the solutions listed in Table 1, the pH values of D100 and D300 are 3.83 and 3.29, respectively, indicating that these two soil solutions are strongly acidic. Under acidic conditions, the cathodic reaction is accelerated due to the depolarization effect of hydrogen ions, which promotes the electrochemical reaction and consequently increases the corrosion rate of the specimens.

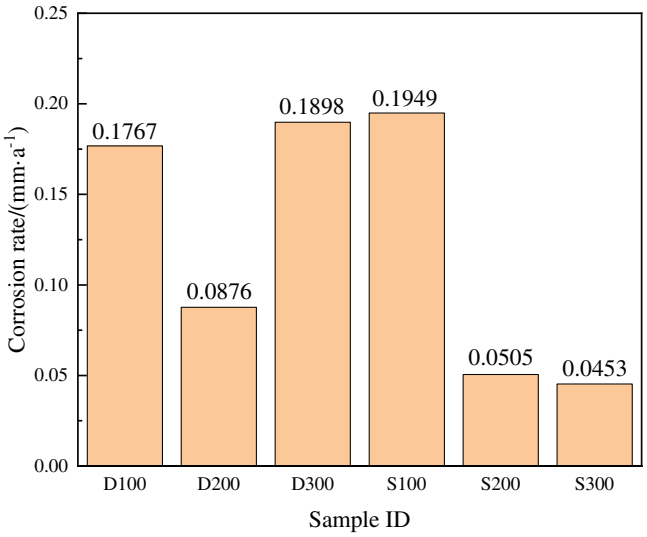


**Figure 2:** Corrosion rates of L415 pipeline steel in six soil-simulated solutions.

In addition, the concentrations of $SO_4^{2-}$ and $NO_3^-$ in the S100 soil solution are significantly higher than those in the other five soil solutions. Soil ions not only participate directly in the electrochemical corrosion reactions but also strongly influence soil resistivity. A higher salt content results in lower resistivity, thereby increasing the corrosivity of the soil environment. Specifically, $Cl^-$ ions promote localized corrosion by penetrating and destabilizing corrosion product films, while $SO_4^{2-}$ ions enhance electrolyte conductivity and facilitate anodic dissolution, particularly under acidic conditions. $NO_3^-$ ions, acting as oxidizing species, can participate in cathodic reactions and increase the corrosion driving force. In contrast, $HCO_3^-$ ions tend to promote the formation of relatively protective corrosion products and thus partially inhibit corrosion.

Fig. 3 shows the corrosion morphologies of the specimens immersed in six soil-simulated solutions. For the steel specimens immersed for 14 days, the surface corrosion product film can be divided into an inner layer and an outer layer. The inner corrosion layer covers almost the entire surface of the pipeline steel substrate, while the outer corrosion layer appears relatively loose. For the specimens exposed to D100, D300, and S100 solutions, although the inner corrosion layer has fully formed, the overall corrosion layers are not compact. A large number of cracks are distributed within the inner layer, and only a small amount of outer corrosion products is sparsely distributed on its surface. These cracks provide pathways for the solution to penetrate through the inner corrosion layer and directly contact the steel substrate, thereby promoting further corrosion. Consequently, the corrosion rates of these three specimens are the highest. In the D200 soil solution, the inner corrosion layer exhibits fewer cracks with reduced crack sizes compared to those in the above three solutions, while the amount of outer corrosion products increases. As a result, the corrosion rate of this specimen is reduced. In contrast, the specimens immersed in S300 and S200 soil solutions show the most compact inner corrosion layers, with almost no visible cracks. The outer corrosion products become denser and interconnected, and in some regions, they completely cover the inner corrosion layer, showing a tendency to form a new dense corrosion layer. The spherical corrosion products observed are identified as $Fe_3O_4$, which possesses low chemical activity and good compactness. This dense corrosion product layer effectively hinders the penetration of the solution to the steel substrate, making further corrosion more difficult. Therefore, the corrosion rates of the specimens in these two solutions are among the lowest of all six groups.

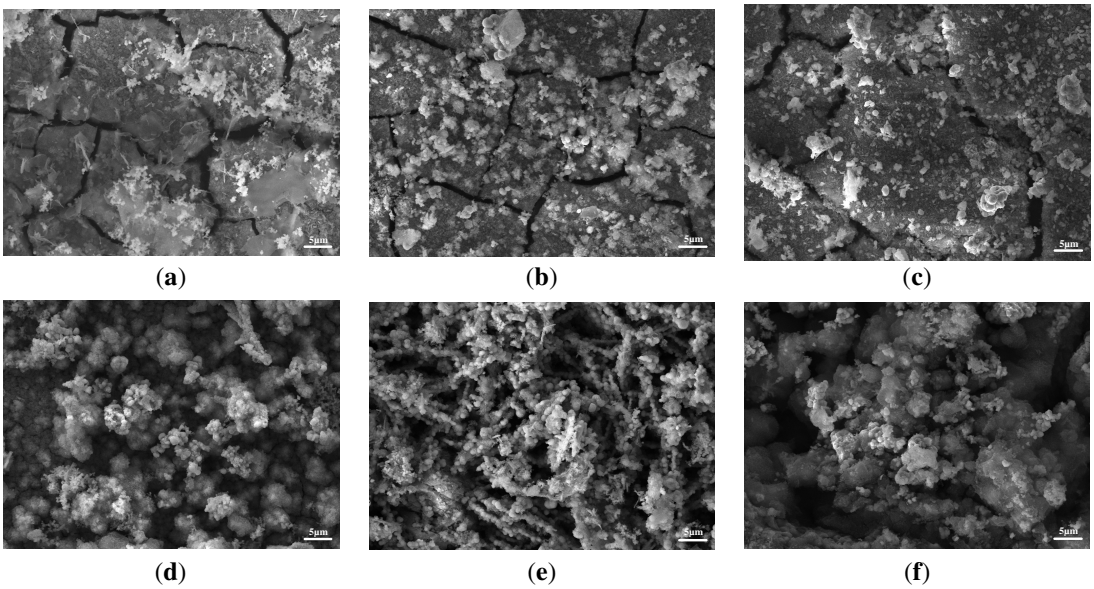


**Figure 3:** Corrosion morphologies of L415 pipeline steel in six soil-simulated solutions: (**a**) S100, (**b**) D300, (**c**) D100, (**d**) D200, (**e**) S200, and (**f**) S300.

### *3.2 Corrosion Product Analysis*

Fig. 4 presents the XRD patterns of the corrosion products formed on L415 pipeline steel specimens immersed in the D300 and S200 soil-simulated solutions. As shown in the figure, the corrosion products formed in the two soil environments are similar, consisting mainly of $Fe_3O_4$ and FeOOH. The inner corrosion layer of the pipeline steel is primarily composed of these two corrosion products. In contrast, the corrosion products formed in the S200 solution contain small amounts of $Fe_2O_3$ and $Fe(OH)_3$. These two compounds are intermediate products formed during the corrosion process of steel and exhibit relatively poor stability. They are mainly distributed in the outer corrosion layer. The corrosion of L415 pipeline steel in the six soil-simulated solutions is an electrochemical process. Since all six soil solutions are acidic and contain a large concentration of $H^+$ ions, the anodic reaction involves the dissolution of iron, while the cathodic reactions include hydrogen evolution and oxygen reduction. The $Fe^{2+}$ ions produced by the anodic reaction combine with $OH^-$ ions generated from the cathodic reactions to form $Fe(OH)_2$. The specific reactions are expressed as follows:

Cathodic reaction:

$$2H^+ + 2e^- \rightarrow H_2 \uparrow \quad (2)$$

$$O_2 + 2H_2O + 4e^- \rightarrow 4OH^- \quad (3)$$

Anodic reaction:

$$Fe - 2e^- \rightarrow Fe^{2+} \quad (4)$$

Corrosion product:

$$Fe^+ + 2OH^- \rightarrow Fe(OH)_2 \quad (5)$$

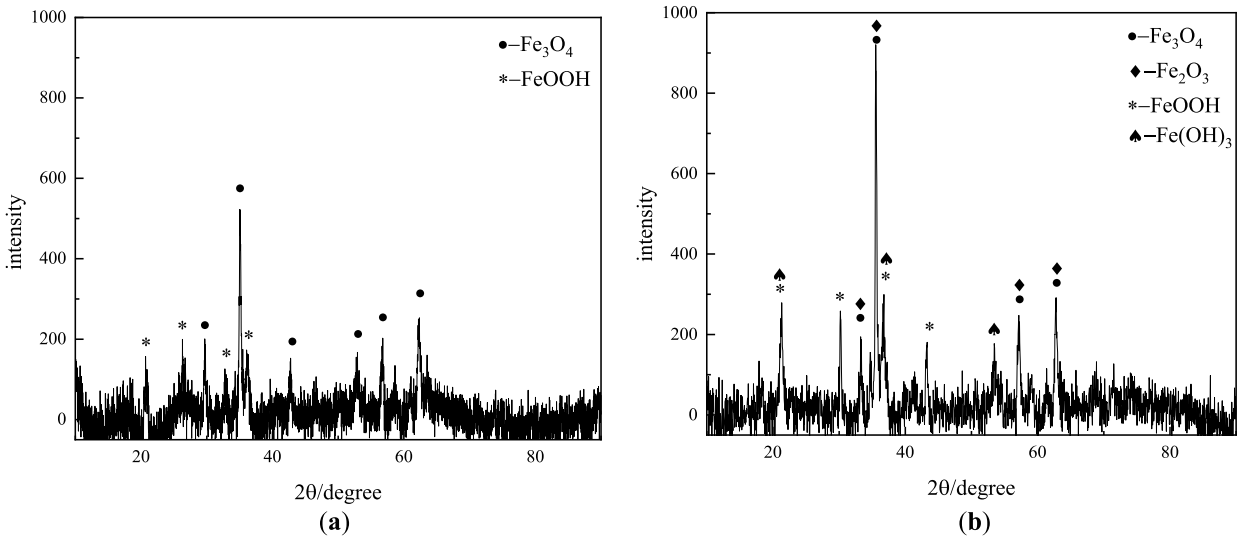


**Figure 4:** XRD patterns of corrosion products formed on L415 pipeline steel in D300 and S200 soil-simulated solutions: (**a**) D300, (**b**) S200.

The above reactions represent the initial corrosion processes occurring at the early stage of contact between the specimens and the solutions. The sparingly soluble corrosion product $Fe(OH)_2$ formed during this stage is thermodynamically unstable. Part of $Fe(OH)_2$ is further oxidized to $Fe(OH)_3$ and subsequently transformed into $Fe_2O_3$, while another portion is oxidized to FeOOH.

$$4Fe(OH)_2 + O_2 + 2H_2O \rightarrow 4Fe(OH)_3 \quad (6)$$

$$2Fe(OH)_3 \rightarrow Fe_2O_3 + 3H_2O \quad (7)$$

$$4Fe(OH)_2 + O_2 \rightarrow 4FeOOH + 2H_2O \quad (8)$$

Previous studies have shown that the FeOOH formed through the above reactions is mainly $\gamma$-FeOOH. Both $\gamma$-FeOOH and $Fe_2O_3$ are high-valence iron oxides and act as effective oxidizing agents. In the presence of $H^+$ ions, they can further react with the iron substrate, promoting their transformation into more thermodynamically stable phases, namely $\alpha$-FeOOH and $Fe_3O_4$.

$$3Fe_2O_3 + Fe + 2H^+ \rightarrow 2Fe_3O_4 + 2Fe^+ + H_2O \quad (9)$$

$$\gamma - FeOOH + H^+ + e^- \rightarrow Fe_3O_4 + 2H_2O \quad (10)$$

$$\gamma - FeOOH \rightarrow FeO_X(OH)_{3-X} \rightarrow \alpha - FeOOH \quad (11)$$

Throughout the corrosion process of L415 pipeline steel, although the final corrosion products are relatively stable and can adhere to the steel surface to retard further corrosion, the acidic soil environment promotes hydrogen evolution during the cathodic reaction. The generated hydrogen gas diffuses outward from the steel surface and penetrates through the corrosion product layer, leading to the formation of cracks and a loosening of the corrosion layer structure. Moreover, in order to reach a more stable state, the intermediate corrosion products further react with $H^+$ ions in the solution and with the steel substrate, which accelerates the corrosion process. Consequently, a lower pH results in the formation of looser and less protective corrosion product layers, thereby providing weaker protection to the steel substrate.

### *3.3 Polarization Curve Analysis*

Fig. 5 shows the polarization curves of L415 pipeline steel after immersion in different soil-simulated solutions for 14 days. As illustrated in the figure, no passivation behavior is observed in the anodic region of the polarization curves in any of the soil solutions, indicating that the corrosion process is dominated by active dissolution. In the cathodic region, two inflection points are observed at low potentials and near the corrosion potential, suggesting the coexistence of hydrogen depolarization corrosion and oxygen reduction reactions. Table 2 lists the electrochemical parameters obtained by fitting the polarization curves using the Tafel extrapolation method. According to Faraday's law, a higher corrosion current density corresponds to a higher corrosion rate and more severe corrosion. It can be observed that the corrosion current densities of L415 pipeline steel are relatively high in the S100, D300, and D100 soil solutions, followed by the D200 solution, while much lower values are obtained in the S200 and S300 solutions. Specifically, the corrosion current density in the S100 solution is 5.33 times that in the S300 solution. This trend is in good agreement with the corrosion rate results obtained in the six soil-simulated solutions.

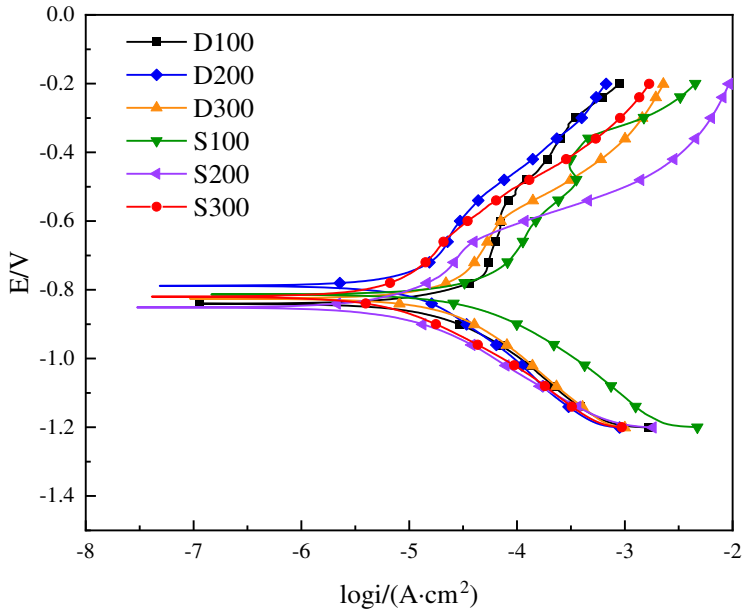


**Figure 5:** Polarization curves of L415 pipeline steel after immersion in different soil-simulated solutions for 14 days.

**Table 2:** Electrochemical parameters obtained from Tafel plots for L415 steel.

| Solution ID | $E_{corr}$ (V vs. SCE) | $i_{corr}$ (A·cm$^{-2}$) |
|---|---|---|
| D100 | −0.84 | $2.37 \times 10^{-5}$ |
| D200 | −0.788 | $1.66 \times 10^{-5}$ |
| D300 | −0.825 | $2.76 \times 10^{-5}$ |
| S100 | −0.814 | $4.07 \times 10^{-5}$ |
| S200 | −0.851 | $7.96 \times 10^{-6}$ |
| S300 | −0.82 | $7.63 \times 10^{-6}$ |

### *3.4 Electrochemical Impedance Spectroscopy Analysis*

Fig. 6 shows the electrochemical impedance spectra of L415 pipeline steel in six soil-simulated solutions. In Fig. 6a, the Nyquist plot of the specimen immersed in the S300 soil solution consists of two capacitive arcs, one small and one large, indicating relatively low conductivity of the solution and the presence of dispersion effects. In contrast, the Nyquist plots of the specimens in the other five soil solutions exhibit a single capacitive arc, suggesting that the electrochemical behavior of the electrode is mainly controlled by charge transfer processes and the resistance and capacitance of the corrosion product film. The radius of the capacitive arc reflects the stability of the corrosion product film. A larger arc radius indicates a stronger hindrance to charge transfer and, consequently, better corrosion resistance of the specimen.

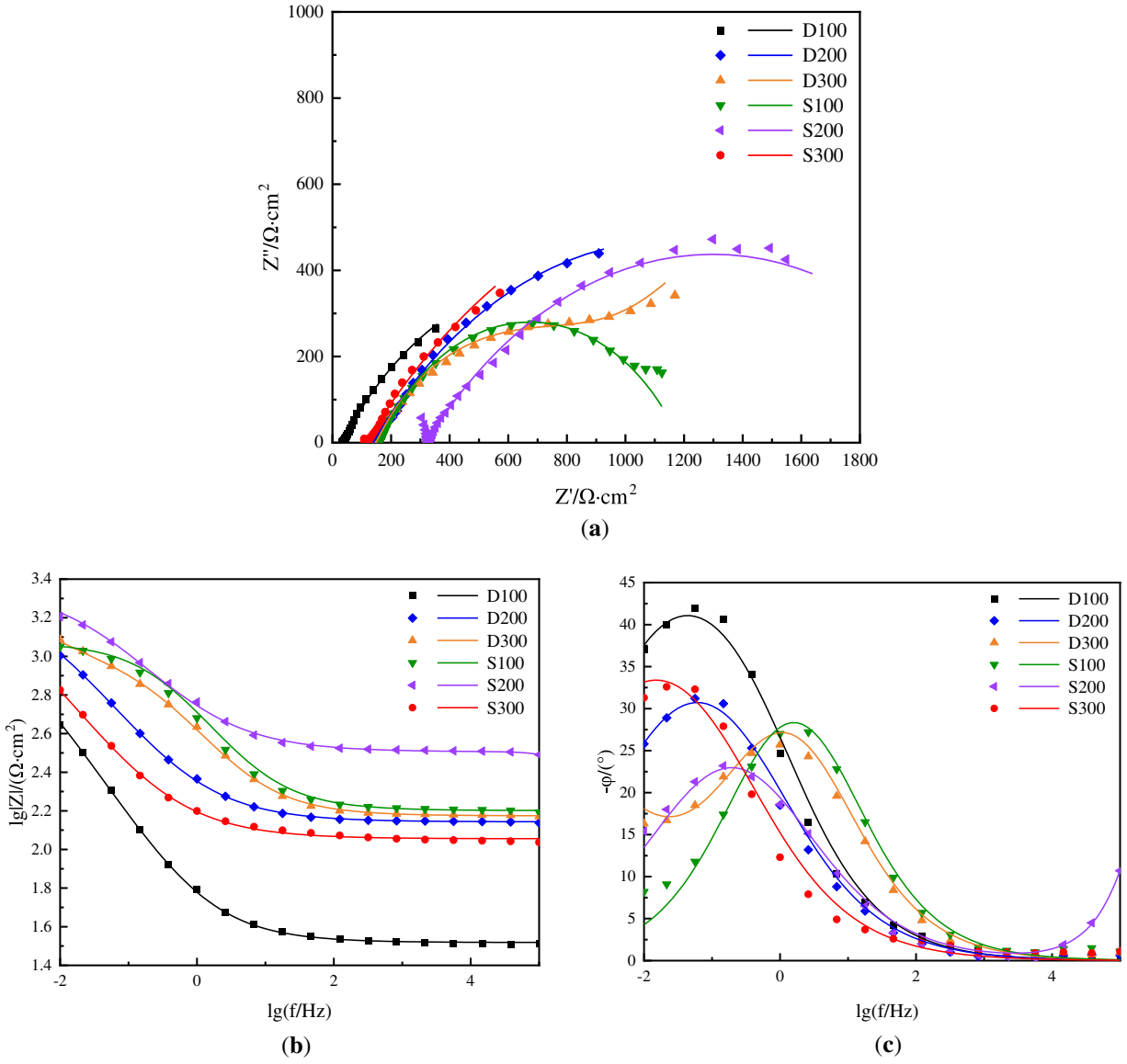


**Figure 6:** EIS spectra for L415 steel in the four simulated soil solutions: (**a**) Nyquist plots, (**b**,**c**) Bode plots.

As shown in Fig. 6b, the impedance modulus in the low-frequency region represents the total resistance of the corrosion system, including both the polarization resistance and the solution resistance, whereas the

impedance modulus in the high-frequency region corresponds to the solution resistance. In Fig. 6c, the phase angle ($\theta$) values in all six soil solutions are greater than zero. Two phase-angle peaks are observed for the specimen in the S300 soil solution, while only one peak is present for the specimens in the other soil solutions. The peaks appearing in the Bode phase plots correspond well to the capacitive arcs observed in the Nyquist plots.

Fig. 7 shows the equivalent electrical circuit used to fit the electrochemical impedance spectra, and the fitted parameters are listed in Table 3. In the equivalent circuit, $R_s$ represents the solution resistance between the specimen and the reference electrode. $Q$ denotes the constant phase element (CPE), where $Q_c$ corresponds to the capacitance of the corrosion product film on the specimen surface, and $Q_{dl}$ represents the double-layer capacitance at the interface between the specimen surface and the solution. $R_c$ is the resistance of the corrosion product film, and $R_{ct}$ is the charge transfer resistance associated with the electrochemical reaction process.

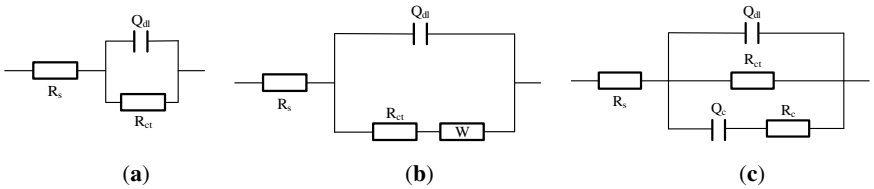


**Figure 7:** Equivalent circuit diagrams of L415 pipeline steel in different simulated soil solutions: (**a**) D100, D200, S100, S300; (**b**) D300; (**c**) S200.

**Table 3:** Fitted electrochemical impedance spectroscopy (EIS) parameters.

| Solution ID | $R_s/(\Omega\cdot cm^2)$ | $Q_c/(F\cdot cm^{-2})$ | $R_c/(\Omega\cdot cm^2)$ | $Q_{dl}/(F\cdot cm^{-2})$ | $R_{ct}/(\Omega\cdot cm^2)$ | $R_p/(\Omega\cdot cm^2)$ |
|---|---|---|---|---|---|---|
| D100 | 32.99 | / | / | $9.75 \times 10^{-3}$ | 1504 | 1504 |
| D200 | 139.1 | / | / | $3.29 \times 10^{-3}$ | 2042 | 2042 |
| D300 | 149.4 | / | / | $8.45 \times 10^{-4}$ | 863 | 863 |
| S100 | 158.7 | / | / | $6.15 \times 10^{-4}$ | 1031 | 1031 |
| S200 | 104.3 | $2.10 \times 10^{-7}$ | 2171 | $9.93 \times 10^{-4}$ | 240.3 | 2411 |
| S300 | 113.7 | / | / | $6.57 \times 10^{-3}$ | 2702 | 2702 |

The polarization resistance ($R_p$) is defined as the sum of the charge transfer resistance ($R_{ct}$) and the corrosion product film resistance ($R_c$), and it effectively characterizes the resistance of L415 pipeline steel during the corrosion process. A larger $R_p$ value indicates a lower corrosion rate. As shown in Table 3, the specimen immersed in the S300 soil solution exhibits the highest $R_p$ value, while the lowest $R_p$ is obtained in the S100 soil solution. The overall variation trend of $R_p$ for L415 pipeline steel in the six soil-simulated solutions is consistent with the corrosion rate results. The goodness-of-fit for all fitted spectra reaches the order of $10^{-3}$.

## 4 Conclusions

To investigate the corrosion behavior of L415 pipeline steel in acidic red soil environments of southern Jiangxi, immersion tests and electrochemical measurements were conducted in six simulated soil solutions for 14 days. The main conclusions are as follows:

1. The corrosion rates decreased in the order of S100 > D300 > D100 > D200 > S200 > S300. The highest corrosion rate (S100) was 4.3 times that of the lowest (S300). The differences were mainly governed by solution pH and ion concentration, with lower pH and higher ion concentration leading to more severe corrosion.
2. The corrosion products consisted of an inner layer mainly composed of $Fe_3O_4$ and FeOOH and an outer layer primarily composed of $Fe_2O_3$ and $Fe(OH)_3$. The inner layer was denser and provided better protection to the steel substrate. The corrosion mechanism involved iron dissolution as the anodic reaction and hydrogen evolution and oxygen reduction as cathodic reactions.
3. The highest corrosion current density was observed in S100 ($4.07 \times 10^{-5}$ A·cm$^{-2}$), which was 5.33 times that in S300. In S300, corrosion was influenced by diffusion effects due to lower conductivity, whereas in the other solutions, corrosion was mainly controlled by charge transfer and corrosion product film properties. Electrochemical results were consistent with the measured corrosion rates.

**Acknowledgement:** The authors would like to thank all contributors for their valuable efforts in validation, data curation, manuscript preparation, and project administration, which made this study possible.

**Funding Statement:** This study was supported by the National Natural Science Foundation of China [grant numbers: 62173049].

**Author Contributions:** Validation, Shiyao Zhu; Data curation, Ke Mei and Shiyao Zhu; Writing—original draft, Siwen Liu; Writing—review & editing, Ke Mei and Xuyu Liu; Project administration, Ruiquan Liao; Funding acquisition, Ruiquan Liao. All authors reviewed and approved the final version of the manuscript.

**Availability of Data and Materials:** The data presented in this study are available on request from the corresponding author.

**Ethics Approval:** Not applicable.

**Conflicts of Interest:** The authors declare no conflict of interest.

## References

1. Xue F, Wei X, Dong J, Etim IN, Wang C, Ke W. Effect of residual dissolved oxygen on the corrosion behavior of low carbon steel in 0.1M $NaHCO_3$ solution. J Mater Sci Technol. 2018;34(8):1349–58. doi:10.1016/j.jmst.2017.11.004.
2. Yan M, Sun C, Xu J, Dong J, Ke W. Role of Fe oxides in corrosion of pipeline steel in a red clay soil. Corros Sci. 2014;80:309–17. doi:10.1016/j.corsci.2013.11.037.
3. Zhao W, Zhang H, Zou Y. Effect of ambient atmosphere and temperature on the corrosion resistance of X80 high-deformation pipeline steel in bicarbonate solution. Int J Electrochem Sci. 2017;12(1):679–92. doi:10.20964/2017.01.90.
4. Cole IS, Marney D. The science of pipe corrosion: a review of the literature on the corrosion of ferrous metals in soils. Corros Sci. 2012;56:5–16. doi:10.1016/j.corsci.2011.12.001.
5. Cai Z, Qin Q, Liu Y, Wei B, Zhang N, Xu J, et al. Effects of alternating current on microbiologically synergistic corrosion of pipeline steel X80 applied by elastic stress. Corros Commun. 2024;13:1–16. doi:10.1016/j.corcom.2023.08.001.
6. Xie F, Wang Z, Wang D, Yin S. A synergistic effect of dissolved oxygen, $HCO_3^-$, and $Cl^-$ on the electrochemical corrosion behavior of X70 pipeline steel in the oilfield soil environment. Appl Phys A. 2020;126(11):868. doi:10.1007/s00339-020-03792-z.
7. Xu D, Chen T, Yang G, Sun L, Xu C, Liu C, et al. Insight into the effect of oxygen content on the corrosion behavior of X70 pipeline steel in a typical simulated soil solution by dissolution-diffusion-deposition model. Corros Sci. 2024;240:112478. doi:10.1016/j.corsci.2024.112478.

8. Setiawan AR, Fausia PIU, Jannah M, Ramelan A. Unveiling the combined effects of soil acidity and ammonium sulfate on the corrosion behavior of X60 steel pipelines in Indonesian regions. Trans Indian Inst Met. 2025;78(2):30. doi:10.1007/s12666-024-03508-4.
9. Fu Q, Xu J, Wei B, Qin Q, Gao L, Bai Y, et al. The effect of nitrate reducing bacteria on the corrosion behavior of X80 pipeline steel in the soil extract solution of Shenyang. Int J Press Vessels Pip. 2021;190:104313. doi:10.1016/j.ijpvp.2021.104313.
10. Cao X, Wu T, Liu M, Wang B, Zhang M, Li C, et al. Corrosion behavior of the weld joint of X80 pipeline steel in an acidic red soil. Mater Res Express. 2020;7(3):036527. doi:10.1088/2053-1591/ab71c8.
11. Wei B, Xu J, Qin Q, Fu Q, Bai Y, Yu C, et al. Comparison of AC corrosion of X80 steel in real soil, soil extract solution, and simulated solution. J Mater Eng Perform. 2020;29(8):4967–77. doi:10.1007/s11665-020-05002-6.
12. Wu T, Zhou Z, Xu S, Xie Y, Huang L, Yin F. A corrosion failure analysis of copper wires used in outdoor terminal boxes in substation. Eng Fail Anal. 2019;98:83–94. doi:10.1016/j.engfailanal.2019.01.070.
13. Li H, Wan H, Liu Z, Du C, Liu Y, Li X. Corrosion behavior of L415 natural gas pipeline in high pressure oxygen-enriched and high salt environment. Int J Electrochem Sci. 2017;12(8):6940–51. doi:10.20964/2017.08.51.
14. Wang Y, Li X, Zhang J, Tu Q. Corrosion behavior study and failure time analysis of X65 pipeline steel in near-neutral soil. Sci Rep. 2025;15(1):45200. doi:10.1038/s41598-025-29421-4.
15. Liu W, Xu C, Chen H, Zhang Y. Electrochemical corrosion behavior of X80 pipeline steel in acidic and alkaline soil leachates. Int J Press Vessels Pip. 2026;220:105733. doi:10.1016/j.ijpvp.2025.105733.
16. Ma J, Chen JH, Zhang X, Feng ZH, Li JH. Stress corrosion behavior of B+F dual-phase X80 pipeline steel in different soil environments. Mater Today Commun. 2024;38(3):107811. doi:10.1016/j.mtcomm.2023.107811.
17. Shangguan Y, Liu M, Liu X, Mei K, Shi B, Chen H, et al. Sulfate-reducing bacteria-induced corrosion behavior of L415 pipeline steel in southern Jiangxi. China ACS Omega. 2025;10(42):49591–601. doi:10.1021/acsomega.5c04172.
18. Yang G, Zeng L, Shen H, Cui H, Chen T, Chen Z, et al. Unveiling the corrosion evolution and pitting mechanism of X70 pipeline steel in typical near-neutral/bentonite soil environment. J Mater Sci Technol. 2026;243:149–66. doi:10.1016/j.jmst.2025.05.010.
19. Li Y, Liu L, Wang J, Xu S, Su H, Xie Y, et al. A comparative study on the corrosion behavior of Q235 steel in saturated acidic red and yellow soils. Anti Corros Meth Mater. 2025;72(2):161–9. doi:10.1108/acmm-03-2023-2775.
20. Liu L, Shan X, Bi F, Sun C, Wang M, Tan X, et al. Effect of temperature on the electrochemical corrosion behavior of X52 pipeline steel in NS4 simulated solution. Int J Electrochem Sci. 2025;20(1):100883. doi:10.1016/j.ijoes.2024.100883.
21. Liu Z, Liao W, Wu W, Du C, Li X. Failure analysis of leakage caused by perforation in an L415 steel gas pipeline. Case Stud Eng Fail Anal. 2017;9:63–70. doi:10.1016/j.csefa.2017.07.003.
22. Sun Y, Liu Y, Luan D, Yang Y, Li L, Zhang X, et al. Effect of $CO_2$ pressure on the corrosion behavior of base metal and welded joint of L415 pipeline steel in coalbed methane produced water. Mater Today Commun. 2025;48(8):113677. doi:10.1016/j.mtcomm.2025.113677.
23. Liu W, Bi W, Hu Y, Lu W, Feng W, Wang Y, et al. Influence of initial pH and sulfate-reducing bacteria concentration on the microbiologically influenced corrosion of buried pipeline steel. Mater Corros. 2024;75(9):1193–203. doi:10.1002/maco.202414320.
24. Qi G, Qin X, Xie J, Han P, He B. Electrochemical corrosion behaviour of four low-carbon steels in saline soil. RSC Adv. 2022;12(32):20929–45. doi:10.1039/d2ra03200g.
25. Wang X, Cao G, Wang B, Xing Y, Lu M, Qiao L, et al. Effect of electric-arc-induced ablation on corrosion behavior of pipeline steel under high-voltage direct current interference. Anti Corros Meth Mater. 2022;69(5):481–9. doi:10.1108/acmm-04-2022-2641.
26. Dong L, Qiu Y, Song Q, Gu Y. Effect of direct current on hydrogen permeation behavior of X80 pipeline steel in Shanghai soil solution. Eng Fail Anal. 2023;150(5):107297. doi:10.1016/j.engfailanal.2023.107297.
27. Morcillo M, Chico B, Alcántara J, Díaz I, Wolthuis R, de la Fuente D. SEM/micro-Raman characterization of the morphologies of marine atmospheric corrosion products formed on mild steel. J Electrochem Soc. 2016;163(8):C426–39. doi:10.1149/2.0411608jes.
28. Han W, Pan C, Wang Z, Yu G. A study on the initial corrosion behavior of carbon steel exposed to outdoor wet-dry cyclic condition. Corros Sci. 2014;88:89–100. doi:10.1016/j.corsci.2014.07.031.